**行政院國家科學委員會補助專題研究計畫** **□成果報告**
**■期中進度報告**

# 以電鍍法製作含奈米粒子之金屬微結構的熱膨脹係數及疲勞特性研究(2/3)

計畫類別：■ 個別型計畫　□ 整合型計畫
計畫編號：NSC 97 － 2221 － E － 009 － 020 － MY3
年度執行期間： 98 年 08 月 01 日至 99 年 07 月 31 日
全程執行期間： 97 年 08 月 01 日至 100 年 07 月 31 日

計畫主持人：徐文祥
共同主持人：
計畫參與人員：黃家聖，李毅家，林軒宇

成果報告類型(依經費核定清單規定繳交)：■精簡報告　□完整報告

本成果報告包括以下應繳交之附件：
□赴國外出差或研習心得報告一份
□赴大陸地區出差或研習心得報告一份
■出席國際學術會議心得報告及發表之論文各一份
□國際合作研究計畫國外研究報告書一份

處理方式：除產學合作研究計畫、提升產業技術及人才培育研究計畫、列管計畫及下列情形者外，得立即公開查詢
□涉及專利或其他智慧財產權，□一年□二年後可公開查詢

執行單位：國立交通大學機械系

中　華　民　國　99　年　05　月　29　日

## 中文摘要：

本研究利用彎曲測試的方式，藉由電鍍鎳與電鍍鎳-鑽奈米複材所製成的微懸臂樑，以討論材料的疲勞行為與特性。電鍍鎳基材由於奈米鑽石顆粒的添加，使得電鍍鎳-鑽奈米複材具有較高的楊氏係數；特別是添加較小顆粒的奈米鑽石，其複材楊氏係數的提升更是顯著。根據量測的結果，當所加入的奈米鑽石粒徑從 350nm 減至 50nm，其各所形成的複材楊氏係數相較於純電鍍鎳約有 4.6%與 13.6%的提升。但是，電鍍鎳基材也因為奈米鑽石顆粒的添加，而降低材料本身的延性，進而造成複材疲勞強度的輕微衰減。然而，當所加入的奈米鑽石粒徑從 350nm 減至 50nm，奈米鑽石顆粒則可以更有效地阻止差排運動；特別是在低應力的循環負載下，電鍍鎳-鑽奈米複材具有可以和電鍍鎳相比的疲勞壽命，不會因為奈米鑽石的添加而明顯降低複材的疲勞強度。根據疲勞量測的 S-N 曲線結果，電鍍鎳的疲勞強度為 2.41GPa，而電鍍鎳-鑽奈米複材於 350nm 和 50nm 不同粒徑的添加下，其疲勞強度分別為 2.18GPa 和 2.40GPa。

## 英文摘要：

Employing the bending-test method, a fatigue characterization scheme has been preformed on microsized cantilever-beam specimens made of electroplated Ni and Ni-diamond nanocomposites to investigate the related material behavior and properties thoroughly. Due to the nano-diamond incorporation in the electroplated Ni matrix, the Young's modulus reinforcement of composite can be realized especially for small particle size. According to the measurement results, Ni-diamond nanocomposites with the average particle-diameter of 350nm and 50nm can have around 4.6% and 13.6% Young's modulus enhancement than that of pure electroplated Ni, respectively. Meanwhile, the results also show that Ni-diamond nanocomposite has slightly smaller fatigue strength than that of pure electroplated Ni due to the ductility reduction resulted by the nano-diamonds. Nevertheless, once incorporated diamond particle size is reduced from 350nm to 50nm, it has been found that the nano-diamond particles can effectively hinder dislocation motion so that the fatigue lifetime of Ni-diamond nanocomposite can be comparable with that of pure electroplated Ni without sacrificing its fatigue strength, especially in low stress cycling regime. According to the test results of fatigue lifetime in terms of *S-N* curve, the values of fatigue strength are obtained as 2.41GPa, 2.18GPa, and 2.40GPa for electroplated Ni and Ni-diamond nanocomposites with the average particle-diameter of 350nm and 50nm, respectively.

**關鍵詞：**Fatigue; Young's modulus; Electroplating; Nanocomposite; Thin film; MEMS

## 報告內容：

### 1. Introduction

Previously, we have reported that the electrolytic Ni matrix with the incorporation of nano-diamonds could exhibit higher Young's modulus and coefficient of thermal expansion (CTE) [1, 2]. Via the property modification based on the nanocomposite effects, MEMS devices made of the nanocomposite can have superior performance. For example, electro-thermal microactuator made of the nanocomposite can have lower power, larger output force, and ultimate elongation in comparison with the one made of pure electroplated Ni due to the Young's modulus and CTE enhancement of structural material. Micro-resonator made of the nanocomposite can increase its resonance frequency and make itself practical for electro-mechanical signal processing application to RF system [3]. Therefore, the investigation of fatigue property of the electroplated Ni-diamond nanocomposite is essential for the potential application in the fabrication of microelectromechanical systems (MEMS), where moving components are subjected to cyclic load.

To date, a variety of testing methods have been proposed for the fatigue characterization of microsized material. Among these methods, tension and bending tests are two popular testing schemes. Tension method [4, 5] can extract Young's modulus and fracture strength directly from the measured stress-stain curve. However, once the sample becomes very small only with several millimeters [6], the setup requirements for gripping, aligning, and pulling a tested sample become stringent to the method. In comparison with the tension method, bending method [7, 8] can be free of the issues raised by sample gripping and alignment. Furthermore, bending test only requires smaller loading force than that of tension test to yield tested sample with a deformation large enough for accurate measurement, which makes the method suitable for thin film characterization. Thus, in this study, a fatigue characterization scheme based on the bending-test design is proposed and utilized for the property investigation of the Ni-based nanocomposite in terms of Young's modulus, fatigue life, fatigue strength, and fracture mechanism.

### 2. Experimental setup and test sample design

Fig. 1 shows the scheme of the bending-fatigue test where microsized cantilever-beam specimen is tested in a displacement-control mode. A tungsten micro-probe is controlled by the test machine to cyclically exert a loading force on the free-end of cantilever beam with a fixed vertical displacement [9]. Before sample testing, the contact monitoring between micro-probe and microsized cantilever-beam specimen is detected by the load cell underneath the tested specimen. Through the load cell fixed on a precise x-y table and the charge-coupled device (CCD) system, the micro-probe can accurately be placed on the right load-position of microsized cantilever-beam specimen. In this fatigue test machine, the resolutions of load cell and displacement actuation can be controlled at 0.1mN and 0.1μm, respectively. Fig. 2 shows the scheme of microsized cantilever-beam specimen for bending-fatigue test. A contact hole is introduced in the specimen design as the load-position to fix the micro-probe with specimen for preventing the probe-tip from gliding along the beam during the test [10]. The contact hole, 15μm in diameter, is located on the center line of cantilever beam with 130μm from the root of the beam and 50μm from the free-end. The designed width ($w$) and thickness ($t$) of the microsized cantilever-beam specimen are fixed at 50μm and 15μm, respectively.

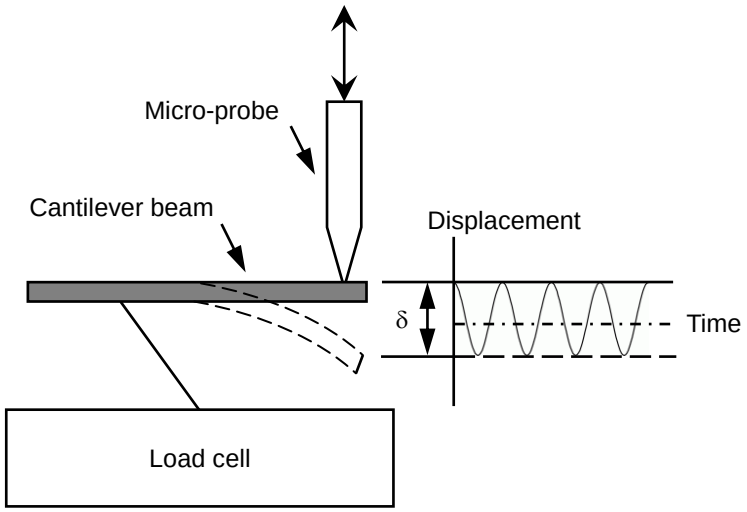


**Fig. 1.** Schematic set-up of the bending-fatigue test for microsized cantilever-beam specimen.

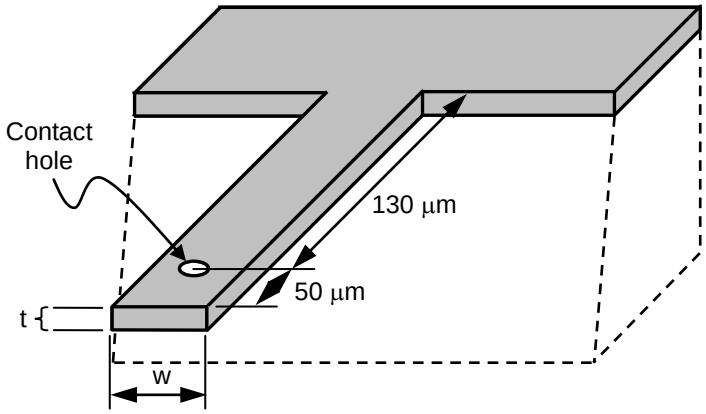


**Fig. 2.** Illustration of microsized cantilever-beam specimen.

The microsized cantilever-beam specimens are fabricated on a silicon substrate as shown in Fig. 3. Initially, the Ti adhesion layer (200Å thick) and Cu seed layer (1000Å thick) are sputtered respectively onto the cleaned silicon wafer. Then, the 20μm thick AZP-4620 photoresister (PR) is spin coated and patterned to form the plating molds of microsized cantilever-beam specimens (Fig. 3(a)). Subsequently, the electroplated Ni-based material is deposited to construct the microsized cantilever-beam specimens (Fig. 3(b)). Table 1 shows the plating bath conditions of electroplated Ni-based materials of pure Ni and Ni-diamond nanocomposites. For the composite-plating of Ni-diamond nanocomposites which are different from pure electroplated Ni, the nano-diamond particles with the average particle-diameters of 350nm and 50nm are added respectively into the different plating baths of sulfuric-based Ni for the co-deposition. And the concentrations of nano-diamond particles in plating baths are all kept at 2g/L. Finally, the fabricated cantilever-beam specimens are released after stripping the plating molds by acetone solution (Fig. 3(c)), which is followed by the removal of silicon underneath using KOH solution (Fig. 3(d)).

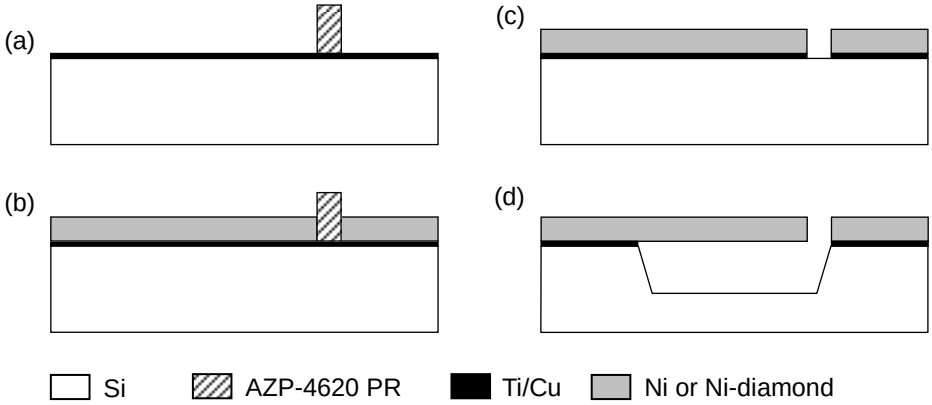


**Fig. 3.** Fabrication process of microsized cantilever-beam specimen.

**Table 1.** Plating bath conditions of Ni-based materials for microsized cantilever-beam specimens.

| | |
|---|---|
| **Ni** | |
| Batch | |
| Nickel sulfamate (g/L) | 400 |
| Nickel chloride (g/L) | 5 |
| Boric acid (g/L) | 40 |
| Wetting agent (c.c.) | 5 |
| pH | 4.1–4.3 |
| Current density (mA/cm$^2$) | 10 |
| Temperature (°C) | 50 |
| **Ni-diamond nanocomposites** | |
| Batch | |
| Nickel sulfamate (g/L) | 400 |
| Nickel chloride (g/L) | 5 |
| Boric acid (g/L) | 40 |
| Wetting agent (c.c.) | 5 |
| Concentration of diamond nanoparticles (g/L) | 2 |
| Average diameter of diamond nanoparticle (nm) | 50, 350 |
| pH | 4.1–4.3 |
| Current density (mA/cm$^2$) | 10 |
| Temperature (°C) | 50 |

Fig. 4 shows the scanning electron microscope (SEM) pictures of as-fabricated cantilever-beam specimens made of electroplated Ni and Ni-diamond nanocomposites for the bending-fatigue test, respectively. According to the elemental analyzer (EA) measurement of the synthesis of Ni-diamond nanocomposites, the diamond content of the corresponding nanocomposite films with the average particle-diameters of 350nm and 50nm are 0.14% and 0.16% in weight fraction, respectively. Furthermore, according to the calculation based on the density of electroplated Ni (8908kg/m$^3$ [1]) and diamond (3510kg/m$^3$ [1]), the diamond content of Ni-diamond nanocomposite films with the average particle-diameters of 350nm and 50nm are 0.35% and 0.41% in volume fraction, respectively.

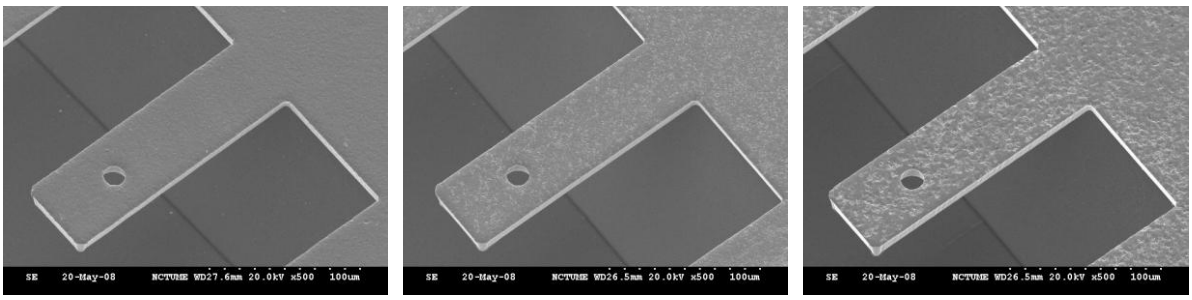

(a) (b) (c)

**Fig. 4.** SEM pictures of as-electroplated cantilever-beam specimens made of: (a) Ni; (b) Ni-diamond nanocomposite with average particle-diameter of 350nm; (c) Ni-diamond nanocomposite with average particle-diameter of 50nm.

## 3. Measurements and results

### *3.1 Static bending test*

Before the test of fatigue lifetime, a static bending test is performed on as-fabricated cantilever nanocomposite beams to determine fatigue-test conditions. Firstly, a tungsten probe tip connected to the test machine is precisely placed at the contact hole of the beams, and the loading force applied by the probe to the beam is measured by a load cell connected to the computer. The tested beam is then gradually deflected by the probe-tip from 0 to 50μm with a displacement step of 2μm. Thus, the loading force versus corresponding displacement can be recorded by the load cell as shown in Fig. 5, which is force-displacement ($F$-$\delta$) curve. As the fatigue-test condition in this study, the maximum displacement loading ($\delta_{max}$) range is determined by the proportional limit of $F$-$\delta$ curve. In this range, the force is proportional to the specimen defection. As shown in Fig. 5, the $\delta_{max}$ are determined as 18μm, 22μm, and 18μm for the electroplated Ni beam and the Ni-diamond nanocomposite beams where the average particle-diameters of nano-diamonds are 350nm and 50nm, respectively.

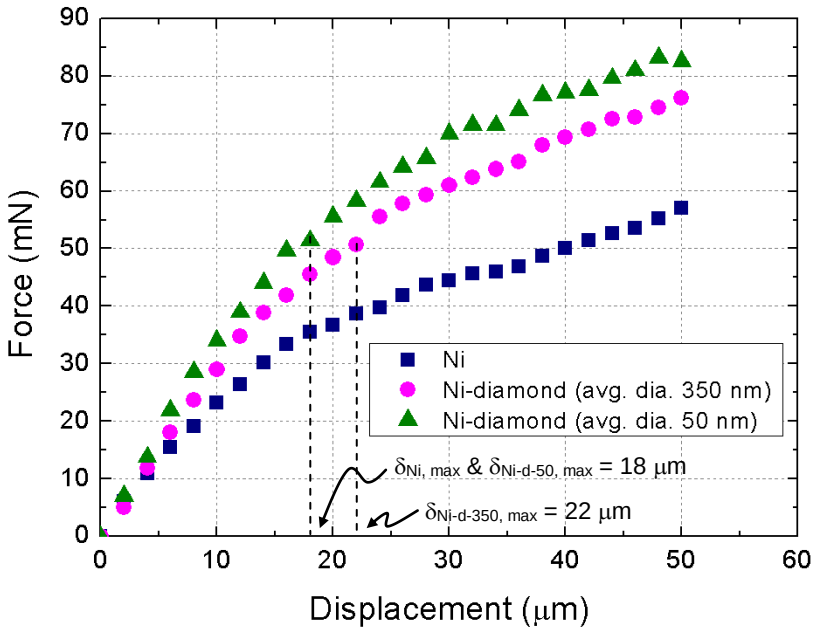


**Fig. 5.** Force-displacement ($F$-$\delta$) curve of microsized cantilever-beam specimens made of the electroplated Ni and Ni-diamond nanocomposites from the static bending tests.

### *3.2 Young's modulus measurement*

According to Fig. 5, the slope of $F$-$\delta$ curve also indicates that the incorporation of nano-diamonds in Ni matrix can enhance the stiffness (force/displacement) of specimen than that of

pure electroplated Ni. Using these stiffness data, the Young's modulus of specimen material can be extracted from the following cantilever-beam equation:

$$E = \frac{L^3}{3I} \cdot \frac{F}{\delta} \quad (1)$$

where $L$ is the length from the beam-root to the load-position, and $I$ is the moment of inertia. Because the equation is only built for idea case without considering actual boundary conditions like quarter-plane and undercut [11] which usually occur in wet-etching process, the extracted Young's modulus becomes unreasonable. In order to solve this problem, commercial finite-element-analysis (FEA) software, ANSYS, is employed to estimate the accurate Young's modulus of the tested samples. Through the construction of $F$-$\delta$ curve analyzed by ANSYS based on the actual parameters of beam size and undercut size, the stiffness can be simulated and compared with the experimental stiffness calculated from data in Fig. 5. Once the analytical data is matched with the experimental one, the corresponding of Young's modulus values can be obtained as 156.9GPa, 165.9GPa, and 178.2GPa for the electroplated Ni and Ni-diamond nanocomposites with the average particle-diameter of 350nm and 50nm, respectively. To further examine the derived Young's modulus values from FEA, the analyzed Young's modulus values of the electroplated films and the resonant frequencies of the tested beams are also compared with the data measured by nanoindenter [12] and LDV resonant frequency measurement method [13], respectively. Table 2 lists the measured Young's modulus values from nanoindenter and resonance methods which well agree with the results of FEA. It is noted that Ni-diamond nanocomposites with the average particle-diameters of 350nm and 50nm both have Young's modulus values which are about 4.6% and 13.6% larger than that of pure electroplated Ni, respectively.

**Table 2.** Young's modulus values of the electroplated films of Ni and Ni-diamond nanocomposites measured by FEA, nanoindenter, and resonance methods.

| | **FEA** | **Nanoindenter** | **Resonance** |
|---|---|---|---|
| **Ni** | 156.9GPa | 156.7±5GPa | 158.1±2GPa |
| **Ni-diamond (avg. dia. 350 nm)** | 165.9GPa | 164.0±5GPa | 163.3±2GPa |
| **Ni-diamond (avg. dia. 50 nm)** | 178.2GPa | 178.0±5GPa | 178.2±2GPa |

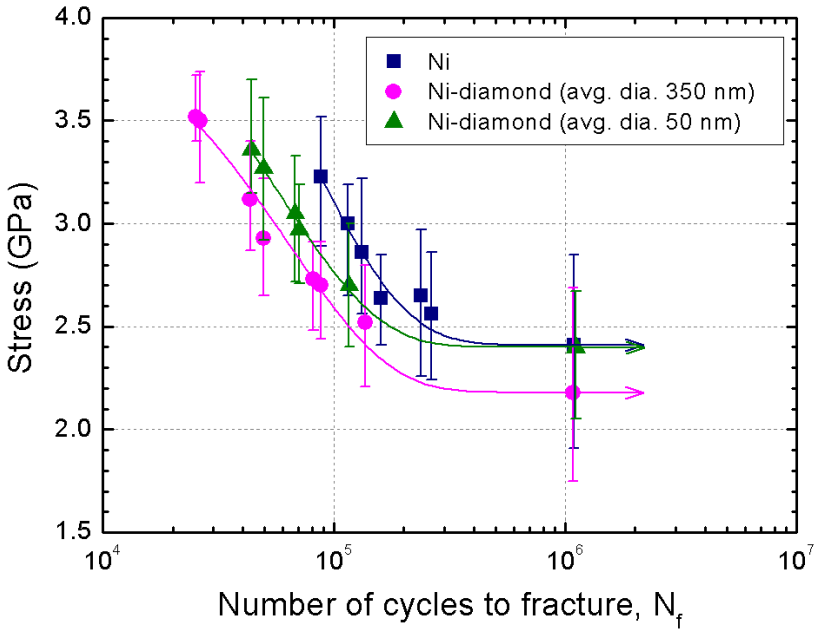


**Fig. 6.** *S-N* curve of microsized cantilever-beam specimens made of the electroplated Ni and Ni-diamond nanocomposites from the fatigue life tests.

*3.3 Fatigue-lifetime test*

As aforementioned in Section 2, the fatigue-lifetime test of the beams made of electroplated Ni and Ni-diamond composites are performed using a micro-probe controlled by the test machine to cyclically apply a sinusoidal displacement on the free-end of cantilever beam with a frequency of 20Hz. Fatigue lifetime is obtained from different cyclic displacement loadings which are below $\delta_{max}$ for each fatigue test condition. Besides, all of the lifetime testes are performed in air and at room temperature. Fig. 6 shows the result of fatigue-lifetime tests in terms of *S*-*N* curve. The *S*-*N* curve, a plot of loading stress (*S*) versus the number of cycles to fracture (*N*) is generally utilized for presenting fatigue data. The values of stress amplitude used in the *S*-*N* curve are evaluated by FEA from the cyclic displacement loading, as shown in Fig. 7 [14, 15] at the root corner with the maximum stress. In the *S*-*N* curve of Fig. 6, each data point is determined while the specimen is broken as shown in Fig. 8, where the loading force detected by the load cell will become diminutive and the number of cycles to fracture will be recorded, simultaneously. In general, fatigue strength is defined as a stress value where the specimen has no failure after $10^6$ cycles [16]. Therefore, as shown in Fig. 6, the fatigue strengths are obtained as 2.41GPa, 2.18GPa, and 2.40GPa for the electroplated Ni, the Ni-diamond nanocomposite incorporated with 350nm in diameter nano-diamond powders, and the one with 50nm in diameter nano-diamond powders, respectively. Meanwhile, it is found that the fatigue strength of Ni-diamond nanocomposite can have 10% increase with the reduction of nano-diamond particle size from 350nm to 50nm, and the fatigue lifetime of Ni-diamond nanocomposite with the average particle-diameter of 50nm would be the same as that of pure electroplated Ni in the low loading stress regime.

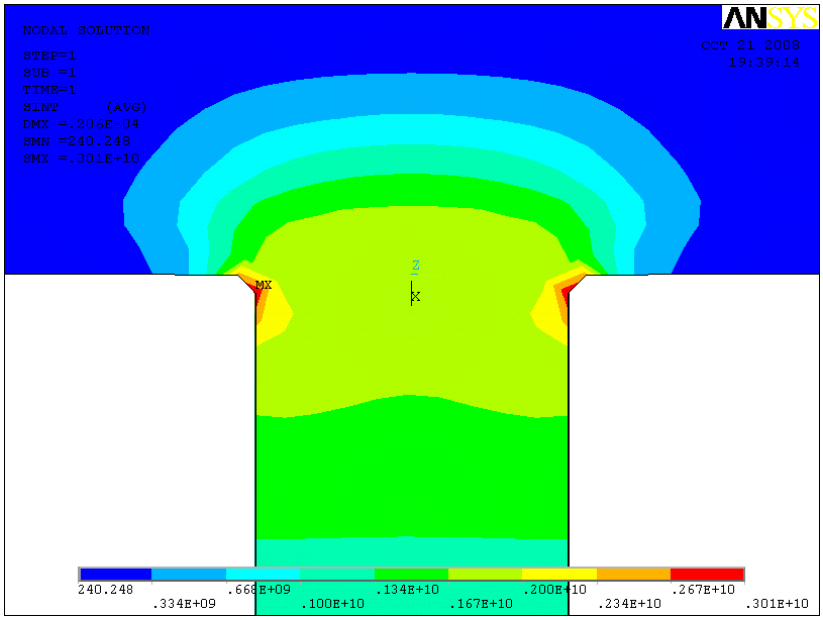


**Fig. 7.** FEA calculated stress-distribution of specimen under the cyclic displacement loading.

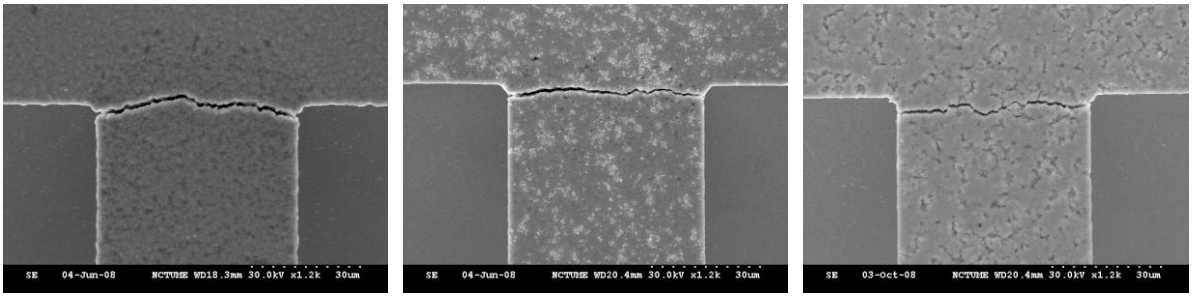


(a) (b) (c)

**Fig. 8.** SEM pictures of electroplated specimen appearance after fatigue fracture: (a) Ni; (b) Ni-diamond nanocomposite with average particle-diameter of 350nm; (c) Ni-diamond nanocomposite with average particle-diameter of 50nm.

## 4. Discussions

Fatigue of ductile material is generally attributed to cyclic plastic deformation involving dislocation motion. The motion would result in the alternating, blunting, re-sharpening, and advancing of a crack tip in a material [17]. From the FEA calculated stress distribution in Fig. 7, it can be found that the maximum stress value is concentrated at the root-corner of cantilever beam. Under cyclic stress loading, crack tip will occur initially at the stress-concentrated zone such as the root-corner of specimen, as shown in Fig. 9(a). Then, the cracks will grow from two ends of the root-corner of specimen (Fig. 9(b)). Finally, the beam will fracture as soon as two ends meet together (Fig. 9(c)). Fig. 10 shows the SEM picture of fatigue fracture interface of Ni-based beam. The cup-cone fracture morphology is a typical ductile characteristic of metal-based material. Fig. 6 has shown that electroplated Ni-diamond nanocomposites have slightly smaller fatigue lifetime than that of pure electroplated Ni especially for larger size particles. It can be attributed to the ductility reduction by incorporation of second-phase particles. As shown in Fig. 10(a) and 10(b) which are the fatigue fracture interface of the pure Ni and the Ni-diamond nanocomposite with the average particle-diameter of 350nm, respectively, the cup-cone has been become finer and the interface morphology has become toward to brittle fracture. In the nanocomposite system, nano-diamond is a source to generate dislocation but also a barrier to block dislocation motion because of the high hardness of diamond. Due to aggravated multiplication and motion hindrance of dislocations in the composite system, crack and void would be easily formed and make the material become brittle. Thus, both the fatigue lifetime and strength of Ni-diamond nanocomposite will degrade and become worse than that of pure electroplated Ni.

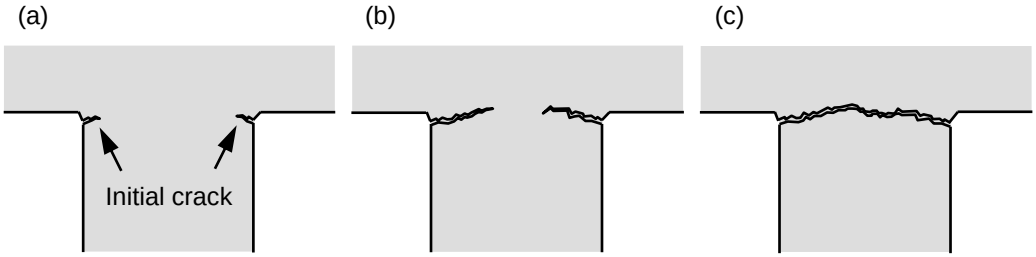


**Fig. 9.** Schematic process of fatigue fracture on microsized cantilever-beam specimen: (a) crack initiation; (b) crack growth; (c) specimen failure.

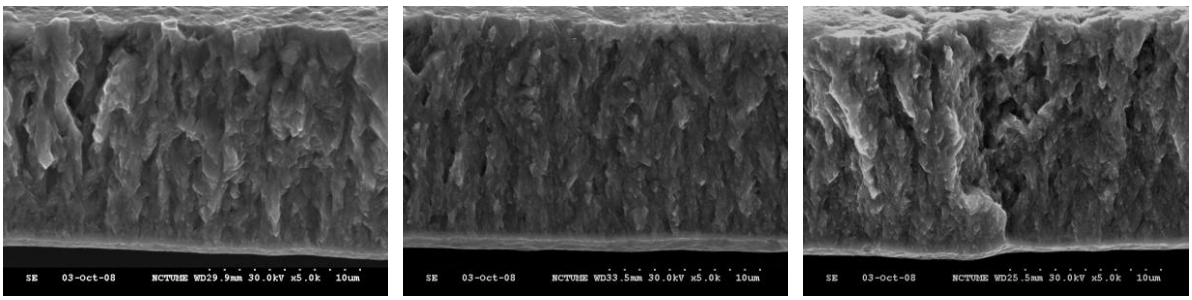

(a) (b) (c)

**Fig. 10.** SEM pictures of cross-sectional morphology of electroplated specimen after fatigue test (~3GPa stress amplitude): (a) Ni; (b) Ni-diamond nanocomposite with average particle-diameter of 350nm; (c) Ni-diamond nanocomposite with average particle-diameter of 50nm.

As aforementioned in Section 3.2, the electroplated Ni-diamond nanocomposites have higher Young's modulus values than that of pure electroplated Ni. Such improvement can be attributed to the particle reinforcement in matrix that the diamond has a larger Young's modulus (~1100GPa [18]) than that of pure electroplated Ni (~156.7GPa as measured). According to the rule-of-mixtures equations [19, 20], the Young's modulus of the composite could be estimated as the one just falling

between the upper and lower bounds as follows:
Upper bound based on the assumption that two phases in a composite are arranged in parallel,

$$E_{c,\text{parallel}} = E_m V_m + E_p V_p \quad (2)$$

and lower bound based on the assumption of two in-series phases,

$$E_{c,\text{series}} = \frac{E_m E_p}{E_m V_p + E_p V_m} \quad (3)$$

where $E$ and $V$ denote the Young's modulus and volume fraction, respectively, and the subscripts of $c$, $m$, and $p$ represent composite, matrix, and particle phases. From Eq. (2) and (3), the calculated upper and lower bound values of Young's modulus are 157.2GPa and 160.0GPa for the electroplated Ni-diamond nanocomposites with the average particle-diameter of 350nm, and 157.3GPa and 160.6GPa for the composite one with the average particle-diameter of 50nm, respectively. Therefore, electroplated Ni-diamond nanocomposites will be expected to have a higher Young's modulus value based on the rule-of-mixtures. These calculated Young's modulus values are quite close to the values derived by different methods as listed in Table 2. Nevertheless, it is noted that, the Young's modulus of electroplated Ni-diamond nanocomposite with the average particle-diameter of 50nm has the largest value.

Previous researches [21-23] have observed that the decrease of particle size can have composite materials gain the largest strengthening and hardening effects which also result in the increases of fatigue lifetime and strength. Under the same volume fraction, more and more nano-particles will be introduced in the composite system with a decrease in the grain size of secondary phase. It could complicate the grain boundary system of the composite with different sliding systems which would hinder dislocation motion, make structure hardened, and prevent crack growth. In fact, the strengthening will be especially pronounced in the high cycle fatigue test with the low stress amplitude, as shown in Fig. 6. As the cyclic-loaded-stress amplitude being reduced, the fatigue lifetime of the electroplated Ni-diamond nanocomposite with small particle size of 50nm will approach gradually to the one of pure electroplated Ni. It is because small particle size means dislocations could still cut through or bypass the secondary phase under low cyclic loaded. The cutting through or by-passing behavior will make the fracture more behave like ductile even though the secondary phase could effectively result in the multiplication and motion hindrance of dislocations. The fatigue lifetime and strength of the electroplated Ni-diamond nanocomposite can, therefore, be improved by incorporating small size particles. In fact, the tendency has also been founded in the fracture interfaces, as shown in Fig. 10(a) and 10(c). The cup-cone fracture morphology of Ni-diamond nanocomposite with the average particle-diameter of 50nm appears closely to that of pure electroplated Ni.

In addition, by comparing the Young's modulus values between Table 2 and rule-of-mixtures calculation, it can be found that the effect of particle size is remarkable for Young's modulus improvement with the particle size reduction of nano-diamonds [23]. The strengthening can also be well explained by aforementioned sliding system complication that makes Young's modulus of the Ni-based composite depend on not only volume fraction of nano-diamond particle but also its sizes.

## 5. Conclusions

Fatigue characterizations of electroplated Ni and Ni-diamond nanocomposite including Young's modulus, fatigue life, and fatigue strength, have been performed by employing bending test to microsized cantilever-beam specimens. Experimental results show that Ni-diamond nanocomposite has higher Young's modulus than that of pure electroplated Ni due to the particle reinforcement in matrix, but it has slightly shorter fatigue lifetime and weaker fatigue strength than that of pure electroplated Ni due to the ductility reduction resulted by the nano-diamonds. Nevertheless, once incorporated diamond particle size is reduced from 350nm to 50nm, the fatigue lifetime of Ni-diamond nanocomposite can be improved and its fatigue strength can be as strong as the pure electroplated Ni. These improvements of fatigue lifetime and strength can be attributed to

the particle size effect. Under the same weight fraction, small diamond size means more diamond particles to complicate the composite grain boundary system which will hinder dislocation motion, make structure hardened, and prevent crack growth. Taking advantages of similar fatigue strength as pure Ni, low electroplating temperature (~50°C), and MEMS/CMOS compatible process, the electroplated Ni-diamond nanocomposite with enhanced Young's modulus is expected as an appropriate material for high frequency and moving components of MEMS devices.

**References**


[1] L.N. Tsai, G.R. Shen, Y.T. Cheng, W. Hsu, Performance improvement of an electrothermal microactuator fabricated using Ni-diamond nanocomposite, *J. Microelectromech. Syst.* 15 (2006) pp. 149-158.

[2] L.N. Tsai, Y.T. Cheng, W. Hsu, Nanocomposite Effects on the of Thermal Expansion Modification for High Performance Electro-Thermal Microactuator, in: *Proceeding of IEEE MEMS'05*, Miami, Florida, U.S.A., 2005, pp. 467-470.

[3] Y.C. Lee, L.N. Tsai, Y.T. Cheng, W. Hsu, Performance enhancement of comb drive actuators utilizing electroplated nickel-diamond nanocomposite, in: *Proceeding of Asia-Pacific Conference of Transducers and Micro-Nano Technology (APCOT)*, Singapore, 2006.

[4] H.S. Cho, K.J. Hemker, K. Lian, J. Goettert, G. Dirras, Measured mechanical properties of LIGA Ni structures, *Sensors and actuators A* 103 (2003) pp. 59-63.

[5] D. Son, J. Kim, T.W. Lim, D. Kwon, Evaluation of fatigue strength of LIGA nickel film by microtensile tests, *Scr. Mater.* 50 (2004) pp. 1265-1269.

[6] T. Yi, C.J. Kim, Measurement of mechanical properties for MEMS materials, *Meas. Sci. Technol.* 10 (1999) pp. 706-716.

[7] S. Maekawa, K. Takashima, M. Shimojo, Y. Higo, S. Sugiura, B. Pfister, M.V. Swain, Fatigue Tests of Ni-P Amorphous Alloy Microcantilever Beams, *Jpn. J. Appl. Phys.* 38 (1999) pp. 7194-7198.

[8] S. Johansson, J.Å. Schweitz, L. Tenerz, J. Tirén, Fracture testing of silicon microelements in situ in a scanning electron microscope, *J. Appl. Phys.* 63 (1988) pp. 4799-4803.

[9] H.K. Liu, B.J. Lee, P.P. Liu, Low cycle fatigue of single crystal silicon thin films, *Sensors and Actuators A* 140 (2007) pp. 257-265.

[10] C.J. Wilson, A. Ormeggi, M. Narbutovskih, Fracture testing of silicon microcantilever beams, *J. Appl. Phys.* 79 (1996) pp. 2386-2393.

[11] C. Hsu, C. Tsou, W. Fang, Measuring thin film elastic modulus using a micromachined cantilever bending test by nanoindenter, *J. Micro/Nanolith. MEMS MOEMS* 6 (2007) pp. 033011.

[12] A.C. Fischer-Cripps, *Nanoindentation*, Springer, New York, 1st edn., 2002, pp. 27-30.

[13] L. Kiesewetter, J.M. Zhang, D. Houdeau, A. Steckenborn, Determination of Young's moduli of micromechanical thin films using the resonance method, *Sensors and Actuators A* 35 (1992) pp. 153-159.

[14] K.P. Larsen, A.A. Rasmussen, J.T. Ravnkilde, M. Ginnerup, O. Hansen, MEMS device for bending test measurements of fatigue and creep of electroplated nickel, *Sensors and Actuators A* 103 (2003) pp. 156-164.

[15] S.M. Allameh, P. Shrotriya, A. Butterwick, S.B. Brown, W.O. Soboyejo, Surface topography evolution and fatigue fracture in polysilicon MEMS structures, *J. Microelectromech. Syst.* 12 (2003) pp. 313-324.

[16] J.E. Shigley, C.R. Mischke, R.G. Budynas, *Mechanical Engineering Design*, Mc Graw Hill, New York, 7th ed., 2003, pp. 313-315.

[17] C.L. Muhlstein, E.A. Stach, R.O. Ritchie, Mechanism of fatigue in micron-scale films of polycrystalline silicon for microelectromechanical systems, *Appl. Phys. Lett.* 80 (2002) pp. 1532-1534.

[18] D. Schneider, M.D. Tucker, Non-destructive characterization and evaluation of thin films by laser-induced ultrasonic surface waves, *Thin Solid Films* 290-291 (1996) pp. 305-311.

[19] W.D. Callister Jr., *Materials Science and Engineering*, Wiley, New York, 4th edn., 1996, pp. 513.
[20] C.L. Hsieh, W.H. Tuan, Elastic and thermal expansion behavior of two-phase composites, *Mater. Sci. Eng. A* 425 (2006) pp. 349-360.
[21] Z. Xue, Y. Huang, M. Li, Particle size effect in metallic materials: a study by the theory of mechanism-based strain gradient plasticity, *Acta Mater.* 50 (2002) pp. 149-160.
[22] Q. Zhang, D.L. Chen, A model for predicting the particle size dependence of the low cycle fatigue life in discontinuously reinforced MMCs, *Scripta Mater.* 51 (2004) pp. 863-867.
[23] N. Chawla, C. Andres, J.W. Jones, J.E. Allison, Effect of SiC volume fraction and particle size on the fatigue resistance of a 2080 Al/$SiC_p$ composite, *Metall. Mater. Trans. A* 29 (1998), pp. 2843-2854.

# 將在 APCOT 2010 研討會發表之三篇論文摘要

## 5th Asia-Pacific Conference on Transducers and Micro-Nano Technology
## July 6-9, 2010 - Perth, West Australia

**NSC 97-2221-E-009-020-MY3**

**註：此期中報告繳交時間為五月底，故尚無法附上預訂七月參加之會議心得報告**

# A Rapid Fatigue Test Method on Microstructures

Hsuan-Yu Lin, Yi-Chia Lee*, and Wensyang Hsu
Department of Mechanical Engineering, National Chiao Tung University, Hsinchu, Taiwan
*Corresponding author: Email hook.me94g@nctu.edu.tw

**Abstract:** Fatigue behaviour of thin film is different from the bulk material in general. However, a fatigue test usually takes long time. In this study, an excitation method is proposed to perform rapid fatigue test on microstructure by exciting a cantilever beam at its resonant frequency. With experimentally determined quality factor, the relative displacement between PZT actuator and the test sample can be determined. By controlling the excitation amplitude, the desired stress on sample can be achieved. Single crystal silicon is used here to demonstrate the proposed method. It is found that fatigue stress of single crystal silicon is 1.33GPa after 10e9 cycles. For excitation at 130 kHz, it takes only about 128 minutes to test 10e9 cycles.

**1 Introduction:** Mechanical fatigue is a critical issue in designing a device with movable parts, especially for long-term and repetitive operation. For fatigue tests on microstructures, previous approaches either used external actuators to push specimens [1,2,3], which would require long testing time, or fabricated the test sample with an *in situ* micro actuator [4,5], which would be hard to prepare the sample and control the loading.

In this study, an excitation method is proposed. The test sample is excited by an external actuator at resonant frequency of the test sample. Therefore, a simple test sample, such as a micro cantilever, can be prepared more easily, and fatigue test can be accomplished at suitable stress range rapidly.

**2 Concept:** The test sample here, such as a micro cantilever, is excited by a commercial PZT actuator in out-of-plane direction at resonant frequency, as shown in Fig. 1. With experimentally determined quality factor, Q, the relative displacement between PZT motion and sample can be derived. Then the displacement amplitude of the sample can be controlled at different PZT voltages at resonant frequency to perform fatigue tests. The relation of stress and excitation amplitude in out of plane direction is found to be:

$$\sigma = \frac{3QEt}{2L^2} Y_{.0} \qquad (1)$$

E is Young's modulus. $Y_0$ is excitation amplitude of PZT, t and L are thickness and length of micro cantilever, respectively.

**3 Experiment setup and results:** Here single crystal silicon is used to demonstrate the proposed method because of its high Q factor, micro cantilever beams are fabricated by double-side RIE etching of (100) silicon wafer. Two kinds of Si cantilever beams are fabricated, one is resonated at 130 kHz for low-stress, high-cycle test, and another with plane mass is resonated at 20 kHz for high-stress, low-cycle fatigue test, as shown in Fig.2.

The experiment setup is shown in Fig.3. By using Laser Doppler Vibrometer (LDV) to characterize the Q factor, resonant frequency, and the amplitude, the life cycles of Si cantilevers at different periodic loadings are determined, as shown in Fig. 4. It is found that fatigue stress of single crystal silicon is 1.33GPa at around 10e9 cycles. For excitation at 130 kHz, it takes only about 128 minutes in the proposed method Comparing to fatigue test on a commercial micro testing machine (μMTS), it usually can operate only up to 10 Hz, then it would need more than 1000 days to test 10e9 cycles. More detailed results and discussions will be presented in full paper.

## Acknowledgements

The authors would like to express the appreciations to Nano Facility Center of National Chiao Tung University, Instrument Technology Research Center, and National Chip Implementation Center for the support of the fabrication and measurement instruments. This work is supported by Taiwan National Science Council, NSC 97-2221-E-009-020-MY3.

# Feasibility Study on Using Polymer as Protecting Material in Fabricating Suspended Single-Crystal-Silicon Microstructures

Yu-Hsin Lin[1,2*], and Wensyang Hsu[1]

[1]Department of Mechanical Engineering, National Chiao Tung University, 1001 Ta Hsueh Road, Hsinchu, Taiwan, 30010, R.O.C

[2]Instrument Technology Research Center, National Applied Research Laboratories, 20 R & D Road VI, Hsinchu Science Park, Hsinchu, Taiwan, 30010, ROC

*Corresponding author: yhlin@itrc.org.tw

**Abstract:** This paper presents a rapid bulk micromachining process to fabricate suspended single-crystal-silicon (SCS) microstructures by using polymer as protecting material at both anisotropic etching and isotropic etching steps. Without using $SiO_2$ deposition or Boron doping as protection layer at releasing step, the proposed method can fabricate suspended SCS microstructures by only using Inductively Coupled Plasma Reactive Ion Etching (ICP-RIE), which could simplify fabrication process and save fabrication time. Critical fabrication parameters are systematically investigated to verify the feasibility of the proposed method.

**1 Introduction:** Due to excellent material properties of single-crystal-silicon (SCS), different methods have been developed to fabricate suspended SCS microstructures [1-4]. In deep reactive ion etching (RIE) technique, protecting the silicon sidewall during the releasing process is the critical step to form a suspended SCS microstructure. In technology of Inductively Coupled Plasma Reactive ion etching (ICP-RIE), polymer has been used in the standard Bosch recipe as protecting material to fabricate the high-aspect-ratio microstructures [5] at anisotropic etching step. However, the polymer is a soft material which is difficult to protect long isotropic etching at releasing step. Therefore, $SiO_2$ coating [1-3] and Boron doping [4] have been proposed in previous literatures to protect the silicon during the releasing step in order to form suspended SCS microstructures. However, $SiO_2$ deposition or Boron doping needs additional equipments beside ICP-RIE.

Here, a bulk micromachining method using only ICP-RIE to fabricate suspended SCS microstructures is proposed by using polymer as the protecting material at both anisotropic etching and isotropic etching steps. Key parameters, such as polymer deposition time and thickness at different opening gaps, are experimentally investigated.

**2 Process Flow:** The experimental investigations of the proposed technique are conducted on the STS Multiplex ICP-RIE. Fig.1 schematically shows the fabrication process of suspended SCS microstructures using polymer as protecting material at both anisotropic etching and isotropic etching. Beside the photo-resist (AZ4620) patterning step, as shown in Fig.1(a), all other steps are conducted in the ICP-RIE chamber. After forming high-aspect-ratio trenches by Bosch cyclic anisotropic etching, as shown in Fig.1(b), the critical step is the proper polymer coating in Fig.1(c), which needs to provide sufficient protection on sidewall at base polymer removal step (Fig.1(d)) and isotropic etching step (Fig.1(e)) for releasing suspended SCS microstructures.

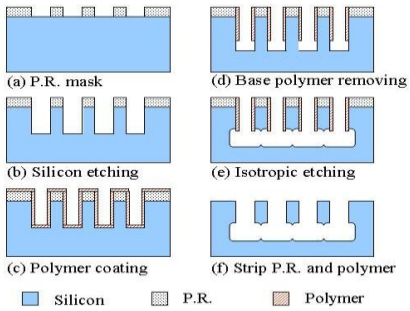


Fig. 1. Fabrication process

**3 Experimental Results and Discussions:** The required polymer deposition time for 30μm deep trench at four different opening gaps has been systematically investigated. The polymer coating recipe is 800/0W source/bias power, 130 sccm $C_4F_8$ flow rate with 5, 15, or 25 minutes deposition time. The opening gaps are 5, 10, 30, and 50μm.

The base polymer removing recipe is 800/12 W source/bias power, 130/13 sccm $SF_6/O_2$ flow rate. The minimum polymer thickness on sidewall (Fig.2a) and maximum polymer thickness on base (Fig.2b) are all measured. Since the residual polymer on the base will affect the following releasing step, it is important to make sure the base polymer is removed completely. Fig.3 shows the etching rate on different base polymer thickness at different gaps.

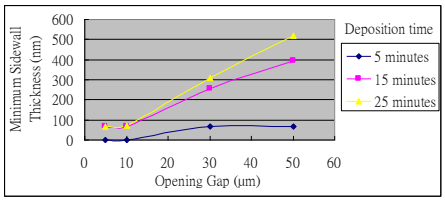


(a)

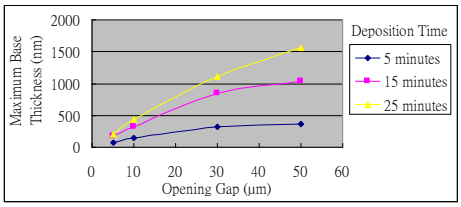


(b)

Fig. 2 Polymer thickness measured (a) on sidewall and, (b) on base of trench structure.

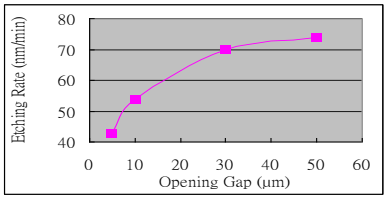


Fig. 3 Etching rate on base polymer

The suitable polymer deposition time and base polymer removing time for successful sidewall protection at isotropic etching for four different gaps are shown in Fig.4. It is found that polymer with 5 minutes deposition is not enough to protect the sidewall well at gaps of 5 and 10 μm.

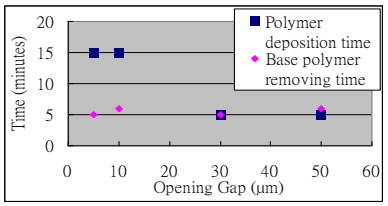


Fig.4 Suitable polymer deposition and base removing time for successful suspended microstructure fabrication

Fig.5 shows the fabrication results of the comb structures without and with proper polymer protection. It can be seen that by just using polymer as protection material at both anisotropic etching and isotropic etching in ICP-RIE, suspended SCS microstructures can be fabricated successfully.

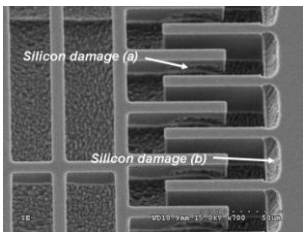


(a)

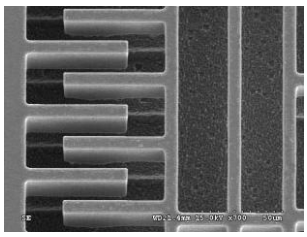

(b)

Fig. 5 Comb structures (a) without proper polymer protection, and (b) with proper polymer protection.

**4 Conclusion:** Feasible recipe by using polymer as protecting material to fabricate suspended SCS microstructures has been successfully identified. Without using $SiO_2$ deposition or Boron doping as protection layer in releasing step, the fabrication can be performed all in the ICP-RIE chamber, which would simplify fabrication process and save fabrication time. More detailed results and discussions will be present in full paper.

## References


N. C. MacDonaid, "SCREAM microelectro-mechanical systems", *Microelectronic Engineering*, vol. 32, pp. 49-73, 1996.

S. Lee, S. Park, and D. Cho, "The surface/bulk micromachining (SBM) process: a new method for fabricating released MEMS in single crystal silicon", *J. Microelectromech. Syst.,* vol. 8, no. 4, pp. 409-415, Dec. 1999.

F. Ayazi, and K. Najafi, "High aspect-ratio combined poly and single crystal silicon (HARPSS) MEMS technology", *J. Microelectromech. Syst.,* vol. 9, no. 3, pp. 77-85, Sep. 2000.

J. Hsieh, and W. Fang, "A boron etch stop assisted lateral silicon etching process for improved high aspect ratio silicon micromachining and its applications", *J. Micromech. Microeng.*, vol. 12, pp. 574-581, 2002.

F. Larmer, and A. Schilp, "Method of anisotropically etching silicon", German Patent DE4241045C1, USA patents 4855017 and 478472

# Output Force Characterization of Scratch Drive Actuators with Flexible Joints

Shawn Chen, Chiawei Chang and Wensyang Hsu*

Department of Mechanical Engineering, National Chiao Tung University 1001 University Road, Hsinchu, Taiwan 300, ROC

*Corresponding author: Email whsu@mail.nctu.edu.tw

**Abstract:** This work presents the design, fabrication and characterization of a low-voltage scratch drive actuator (LVSDA) with flexible joints. Due to a lower flexural rigidity, the driving voltage can be reduced effectively. Here rectangular SDAs made of nickel with and without flexible joints are fabricated by a metal-based surface micromachining process. Flexible joints with different dimensions are also fabricated and tested. Experimental results show that, at the same main plate length (80μm) and width (65μm), the proposed LVSDA can be actuated at 50V, much smaller than 84 V, the minimum required input voltage of the conventional SDA, i.e. without flexible joint design. It is also found that the LVSDA can stretch the attached spring longer than the conventional SDA under the same driving voltage under 100V, which verifies the proposed LVSDA can provide larger output force at lower driving voltage.

**1 Introduction:** The scratch drive actuator (SDA) can yield micro-Newton force and long travel distance with nano-meter step size. It has been adopted in many micro electro-mechanical systems (MEMS), such as self-assembly [1, 2], self-positioning [3], operation of micro cam-motor [4], and actuation of micro-gripper [5]. However, the required driving voltage for SDA is very high, usually between 100 and 200 volts. Here, a flexible joint design is proposed to reduce the required driving voltage of SDA to become a so-called low-voltage scratch drive actuator (LVSDA). The output performances with different flexible joint dimensions are also experimentally characterized.

**2 Concept Design:** The operation of a SDA usually involves charging, pull-in, discharging and one step ahead. In the proposed LVSDA design, flexible joints are incorporated into the main plate structure, as shown in Fig. 1. Therefore, electrostatic force to resist the mechanical force can be reduced. A schematic LVSDA operation cycle is shown in Fig. 2.

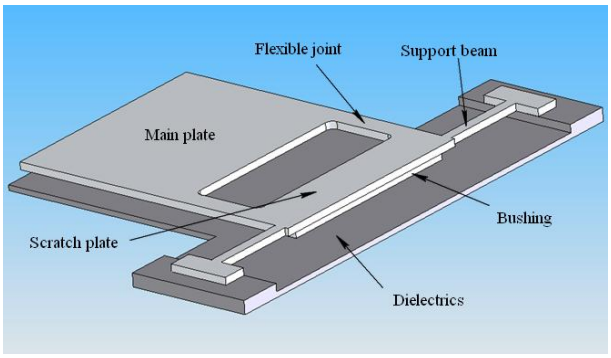


Fig. 1. Concept design of a LVSDA

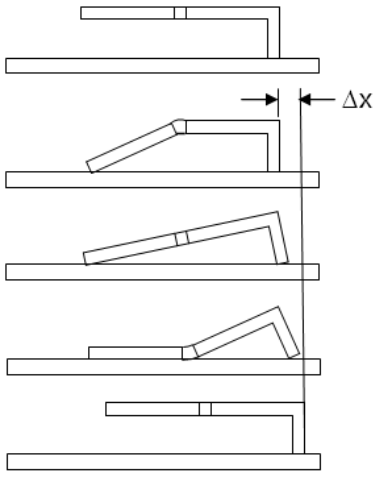


Fig. 2. Operation Principle of LVSDA (a) initial state; (b) charge and pull-in for softer joint; (c) charge and pull-in for stiffer joint; (d) priming; (e) discharge and one step ahead.

**3 Fabrication and Testing:** A two-mask micro electroplating nickel process is used here. Each test sample is composed of four LVSDAs or SDAs with a tether spring attached, as shown in Fig. 3. The length, width, and thickness of main plate are 80 μm, 65μm, and 2.5μm, respectively. Two

different locations of the rectangular hole in the main plate are fabricated. Flexible joints with two different beam widths (3μm and 6μm) are also fabricated and tested. Devices are tested at various sinusoidal pulses of 500Hz. The displacements are recorded under an optical microscope with a CCD camera.

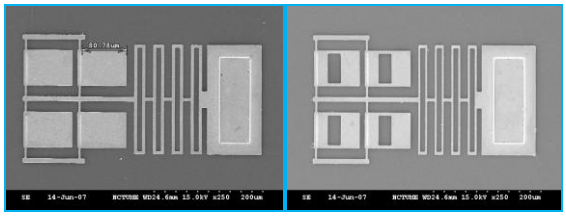

(a) (b)

Fig. 3 Fabricated results. (a)SDA (b) LVSDA

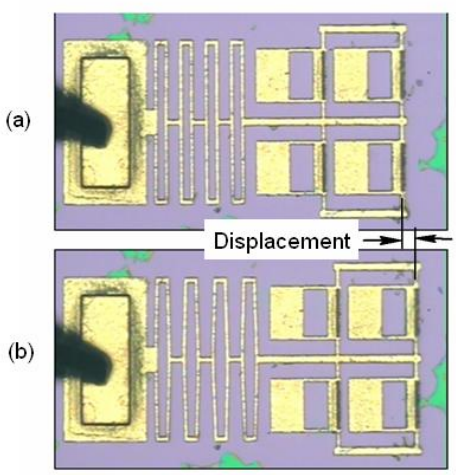


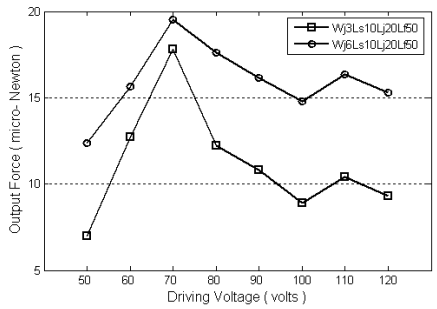


Fig. 4 Displacement test

Fig.5 Output forces with two different Ls

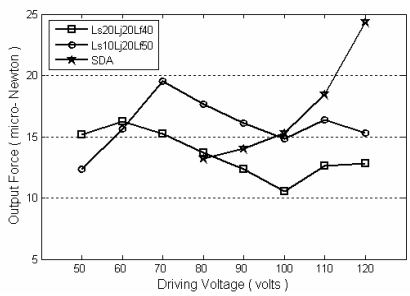


Fig. 6 Output forces with two different flexible beam widths

**4 Results:** Fig.4 shows a typical displacement testing result. With the calculated spring constant, the output forces can be determined from the measured displacement data. The distance of rectangular hole to the bushing is denoted as Ls. Fig. 5 shows the experimental results of output force at different driving voltages with Ls= 10μm and 20μm. It is found that the minimum driving voltage for SDA is around 84V and 50V for LVSDA, respectively. It is also found that shorter Ls can provide larger output force for input voltage higher than 60 V. The output force of LVSDA with Ls=10 reaches its maximum around 70V and remains larger than the output force of SDA until around 97V, which verifies that the proposed LVSDA can provide higher output force at lower driving voltage.

Fig. 6 shows the testing results with two different flexible joint beam widths, Wj, 3μm and 6μm. It can be seen that a wider flexible beam can provide a larger force. More detailed results and discussions will be presented in the final paper.

## Acknowledgements

This work was supported by the National Science Council (Taiwan) under grant NSC 92-2212-E009-035.

## References

[1] T. Akiyama, D. Collard and H. Fujita, “Scratch Drive Actuator with Mechanical Links for Self-Assembly of Three -Dimensional MEMS,” IEEE Journal of Microelectromechanical Systems, vol. 6, 1997, pp.10-17.

[2] C. K. Lee, Y. J. Lai, C. Y. Wu, J. A. Yeh and R. S. Huang, “Feasibility study of self-assembly mechanism for variable optical attenuator,” J. Micromech. Microeng. vol. 15, 2005, pp. 55-62.

[3] R. J. Linderman and V. M. Bright, "Nanometer Precision Positioning Robots Utilizing Optimized Scratch Drive Actuators," Sensors and Actuators: A 91, 2001, pp.292-300.

[4] Y. Kanamori, Y. Aoki, M. Sasaki, H. Hosoya, A. Wada and K. Hane, “Fiber-optical switch using cam-micromotor driven by scratch drive actuators,” J. Micromech. Microeng. vol. 15, 2005, pp. 118-123.

[5] O. Millet, et al.,” Electrostatic actuated micro-gripper using an amplification mechanism,” Sensors and Actuators: A 114, 2004, pp. 371-378.